SHEFEX-3 Optimal Feedback Entry Guidance

Marco Sagliano*, Malak Samaan†, Stephan Theil‡
Deutsches Zentrum für Luft- und Raumfahrt, Robert Hooke Straße 7, Bremen, Germany, 28359
Erwin Mooij§
Delft University of Technology, Kluyverweg 1, 2629, HS Delft, The Netherlands

SHEFEX is a DLR-led series of missions for scientific experiments and reentry technology development. SHEFEX-2 was successfully launched from Norway (Andøya Rocket Range) in June 2012. To go on with the effort to increase the technological level for real space missions, a new challenge in the next years with the development of SHEFEX-3 arises. SHEFEX-3, foreseen to be launched in 2016, will be more complex than SHEFEX-2 in virtue of the presence of a real guided re-entry phase, while for SHEFEX-2 an autonomous Guidance and Control phase was only partially foreseen. As a consequence, the mission will be ambitious, especially in the development of the GNC subsystem. DLR GNC Systems Department will be responsible for the development of Guidance and Navigation modules, while Control will be developed by Airbus Defense and Space, in cooperation with DLR. In this work the development of the nominal entry guidance, based on the use of PseudoSpectral Methods, is discussed. This feedforward control is then coupled with a Gain-Scheduled LQR tracking controller to reduce the error on the terminal points of the mission. Results show that the proposed approach meets the requirements on the physical constraints and the terminal states, satisfying at the same time the strong limitations coming from the need to have a highly-constrained angle of attack profile.

Nomenclature

$\mathbf{A}_k$	k^{th} state matrix
$\mathbf{B}_k$	k^{th} control matrix
$\mathbf{C}_k$	k^{th} output matrix
C_D	Drag coefficient
C_L	Lift coefficient
D	Drag acceleration (m/s^2)
$\mathbf{D}_k$	k^{th} feedthrough matrix
d_{ij}	Coefficient for drag coefficient computation
$\mathbf{e}$	State error
$\mathbf{f}$	Nonlinear system of equations
g	Gravity acceleration (m/s^2)
h	Altitude (km)
h_s	Density Height scale (m)
$\mathbf{I}$	Identity Matrix
J	Cost function
J_2	zonal harmonic
$\mathbf{K}$	LQR Gain Matrix
L	Lift acceleration (m/s^2)

*Research Engineer, Guidance, Navigation and Control Department, AIAA Member
†Research Engineer and Project Manager, Guidance, Navigation and Control Department, AIAA Member
‡Department Head, Guidance, Navigation and Control Department, AIAA Member
§Assistant Professor, Astrodynamics and Space Missions Department, Faculty of Aerospace Engineering, AIAA Associate Fellow

l_{ij}	Coefficient for lift coefficient computation
M	Mach number
m	Mass (kg)
N	Number of sampled points
N_c	Number of controls
N_s	Number of states
n_z	Load factor
$\mathbf{O}$	Zero Matrix
$\mathbf{P}$	Solution of Algebraic Riccati Equation
$\mathbf{Q}$	States Weight Matrix
$\dot{Q}$	Heat Flux (W/m^2)
q	Dynamic pressure (N/m^2)
$\mathbf{R}$	Controls Weight Matrix
r	Radial position (m)
r_e	Earth's equatorial radius (m)
S	Area m^2
T	Temperature (K)
T_h	Temperature gradient (K/m)
t	Time (s)
u_σ	Bank angular velocity (rad/s)
U_v	Controllability condition (m/s^2)
$\mathbf{u}$	Control vector
$\mathbf{u}_c$	Feedback control term
V	Speed (m/s)
w_ϕ	Latitude weight
w_θ	Longitude weight
$\mathbf{x}$	State vector
α	Angle of attack (rad)
γ	Flight-path angle (rad)
$\mu_\oplus$	Earth's gravitational parameter (m^3/s^2)
ϕ	Latitude (rad)
ψ	Velocity-Azimuth Angle (rad)
ρ	Air density (kg/m^3)
θ	Longitude (rad)
$\dot{()}$	first time derivative ()/s)
$\ddot{()}$	second time derivative ()/s^2)
$()_{cur}$	Current value
$()_f$	Final value
$()_{ref}$	Reference value
$()_U$	Maximum value

Abbreviations

KKT	Karush−Kuhn−Tucker
LQR	Linear Quadratic Regulator
LTI	Linear Time Invariant
LTV	Linear Time Variant
NLP	Nonlinear Programming
OCP	Optimal Control Problem
$SHEFEX$	SHarp Edge Flying EXperiment
$SPARTAN$	SHEFEX-3 Pseudospectral Algorithm for Reentry Trajectories ANalysis

I. Introduction

SHEFEX is a DLR-led series of missions for scientific experiments and development of the european technology for atmospheric reentry. SHEFEX-2[1,2] was successfully launched from Norway (Andøya Rocket Range) in June 2012. To go on with the effort to increase the technological level for real space missions, a new challenge in the next years with the development of SHEFEX-3 arises. SHEFEX-3, foreseen to be launched in 2016, will be more complex than SHEFEX-2 in virtue of the presence of a real guided re-entry phase, while for SHEFEX-2 an autonomous Guidance and Control phase was only partially foreseen. As a consequence, the mission will be more complex and ambitious, especially in the development of the GNC subsystem. DLR Guidance, Navigation and Control Systems Department will be responsible for the development of Guidance and Navigation modules, while Control will be developed by Airbus Defense and Space, in cooperation with DLR. In this work the development of the nominal guidance is discussed. The feedforward guidance is described as optimal control problem, which has been transcribed as Nonlinear Programming Problem, and solved with SPARTAN, a tool developed by DLR based on the use of the Flipped Radau Pseudospectral Method. Several constraints are included, both from the physical point of view (limits on load factor, dynamic pressure and heat flux) and from the operational point of view (e.g., actuator saturation). The work is organized as follows. In Section II the SHEFEX-3 mission is described, and the nominal conditions at the entry interface are characterized. Section III reports briefly the mathematical models used for the aerodynamics, the atmosphere and the gravity. In Section IV the Trajectory Planning for SHEFEX-3 is reported in detail, while Section V describes the Trajectory Tracking algorithm. Section VI discusses the results for the nominal trajectory in absence of disturbances, while in Section VII systematic variations on density and aerodynamics are considered. Finally, some future development and conclusions are reported in Section VIII and IX.

Figure 1: SHEFEX-3 Entry vehicle

II. Mission Scenario

SHEFEX-3 is foreseen to be launched in 2016. The current launch site is again Andøya. The spacecraft will be launched with a rocket based on the brazilian engine S-44. After the stages separation, and the coast phase, the unpowered descent phase follows.

Once an altitude of 100 km is reached, the nominal entry phase begins. The entry interface is characterized by a steeper flight-path angle and a lower Mach number w.r.t. the usual entry conditions (for instance, the conditions associated to the reentry from a RendezVous mission with the ISS), which have a higher speed and a smaller magnitude of the flight path angle[4,5] . The mission from the point of view of Guidance terminates with the deployment of the parachute, foreseen to be opened between 5 and 10 km of altitude at a speed between 125 and 185 m/s. The foreseen landing point is Nordaustlandet, one of the biggest islands belonging to the Svalbard archipelago, in Norway. The island has a surface of approximately 14.443 km^2,

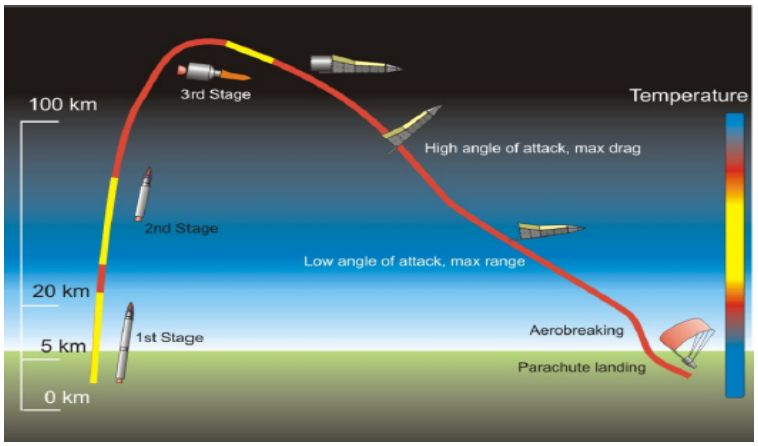

Figure 2: Shefex-3 Mission Profile

and is uninhabited. The nominal entry and terminal conditions are reported in Table 1.

Table 1: Nominal Entry and Terminal Conditions for SHEFEX-3

State	Initial Value	Terminal Value
h (km)	100.1665	7.50 ± 2.50
θ (deg)	19.9826	24.00 ± 1.0
ϕ (deg)	73.6752	79.65 ± 0.3
V (m/s)	3209.6770	155.00 ± 30
γ (deg)	-10.005	free
ψ (deg)	71.2249	free

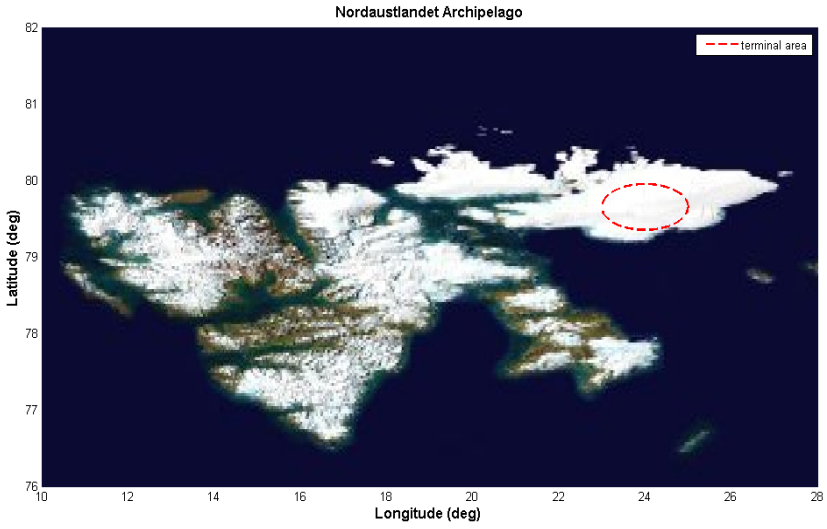

Figure 3: Nordaustlandet - SHEFEX-3 Terminal Area

III. Environmental and aerodynamics models

Earth's atmosphere cannot be perfectly described by analytical expressions. On the other hand, having simplified models, which relate variables like density and temperature are highly desirable, as they represent a powerful tool for preliminary trajectory analysis. In this section the environmental, the aerodynamics models and the angle-of-attack profile implemented are briefly reported.

A. Density

A good analytical approximation of air density is the exponential profile described by

$$\rho(h) = \rho_0 e^{-\frac{h}{h_s}} \tag{1}$$

This profile is of course an approximation, as it would be mathematically associated to an isothermal model. It is usually used from 0 to 86 km, but its use is often extended to the range of $[0, 120]$ km. The height scale h_s is equal to $7.2543 \cdot 10^3$ m.

B. Temperature

The temperature model should be theoretically consistent with the model describing the density and the pressure. That is the isothermal model. However the temperature is often approximated by the the junction of a series of piecewise linear functions. Indeed, for each altitude, it can be computed as

$$T(h) = T_{i-1} + T_{h,i-1} \cdot (h - h_{i-1}), \qquad h \in [h_{i-1}, h_i] \tag{2}$$

C. Gravity

Gravity can be in first approximation modeled as a pure central field generated by the mass of a perfect sphere placed in the center of the Earth.

$$g(r) = \frac{\mu_\oplus}{r^2} \tag{3}$$

A better approximation is obtained with the use of the WGS84 model, which takes into account the oblateness of the Earth,[6] via expansion in spherical harmonics. A simplified version is the correction of the gravitational field associated to the use of the J_2 term,

$$g(r, \phi) = \frac{\mu_\oplus}{r^2} \cdot \left[1 + \frac{3}{2} \cdot J_2 \cdot \left(\frac{r}{r_e}\right)^2 \left(1 - 3\sin^2\phi\right)\right] \tag{4}$$

where the gravitational parameter of the Earth $\mu_\oplus$ and the zonal coefficient J_2, are respectively equal to $3986004.418 \cdot 10^8$ km^3/s^2 and $1.0826271 \cdot 10^{-3}$, as reported in the WGS84 model[7] . The radius of the Earth is assumed equal to 6378100 m.

Figure 4 shows the evolution of the atmospheric density, the temperature, and the acceleration profiles associated to the two cited gravity models.

D. Aerodynamics

SHEFEX-3 aerodynamics is described in terms of coefficients of lift and drag as a function of angle of attack and Mach number. To speed up the simulations and to have an analytical description of the database, once the trimming conditions have been generated[8] , the initial look-up tables have been converted into continuous 2D functions using full cubic polynomials. This approach represents an extension of what has already been done for several entry vehicles, such as the X-33[9] .

$$C_L(\alpha, M) = \begin{bmatrix} \alpha^3 \\ \alpha^2 \\ \alpha^1 \\ 1 \end{bmatrix}^T \begin{bmatrix} l_{11} & l_{12} & l_{13} & l_{14} \\ l_{21} & l_{22} & l_{23} & l_{24} \\ l_{31} & l_{32} & l_{33} & l_{34} \\ l_{41} & l_{42} & l_{43} & l_{44} \end{bmatrix} \begin{bmatrix} M^3 \\ M^2 \\ M \\ 1 \end{bmatrix} \tag{5}$$

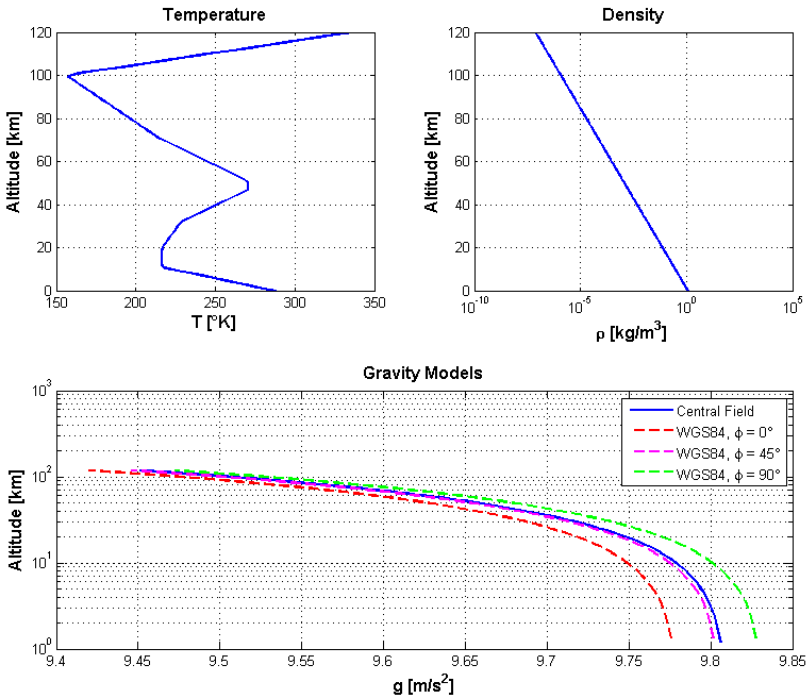

Figure 4: Environmental models

$$C_D(\alpha, M) = \begin{bmatrix} \alpha^3 \\ \alpha^2 \\ \alpha^1 \\ 1 \end{bmatrix}^T \begin{bmatrix} d_{11} & d_{12} & d_{13} & d_{14} \\ d_{21} & d_{22} & d_{23} & d_{24} \\ d_{31} & d_{32} & d_{33} & d_{34} \\ d_{41} & d_{42} & d_{43} & d_{44} \end{bmatrix} \begin{bmatrix} M^3 \\ M^2 \\ M \\ 1 \end{bmatrix} \tag{6}$$

The coefficients l_{ij}, d_{ij} are determined to minimize the error between the look-up tables and the continuous functions representing the aerodynamic coefficients through a least square fit procedure.

E. Angle of attack

The angle of attack is usually an active control variable in the entry problem, together with the bank angle. For SHEFEX-3 it will be considered as a nominal profile in the trajectory planner and as a secondary control variable for tracking purposes. In the nominal scenario it is a given profile characterized by the presence of a high and a low angle of attack phase. These two phases are linked by a transition compatible with the limitations of the flight control system. In particular, the angle of attack is modeled as function of Mach represented by two constant functions joined by a linear transition between the higher and the lower α.

As a consequence, α represents a constraint in the planning phase and a secondary control in the tracking phase. In other words, the possibility to control the vehicle is limited mainly, but not only, to bank-angle modulation.

F. Path and Control Constraints

Other constraints taken into account are the dynamic pressure, the heat flux and the load factor. Moreover, to make the simulations more realistic, further constraints on the bank angle rates are included. In particular, the angular velocity and the angular acceleration are limited. This means that the hypothesis of "inertialess" vehicle is here rejected. All these constraints are listed in Tables 2 and 3.

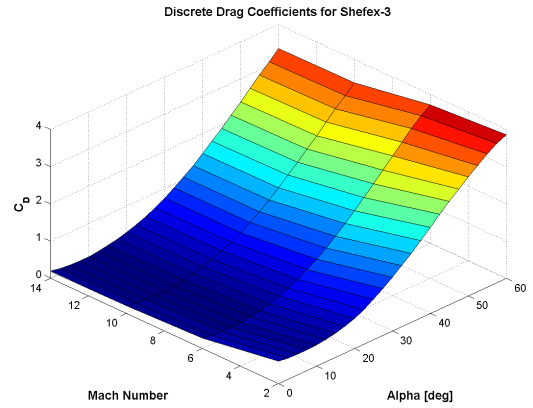

(a) Discrete C_D

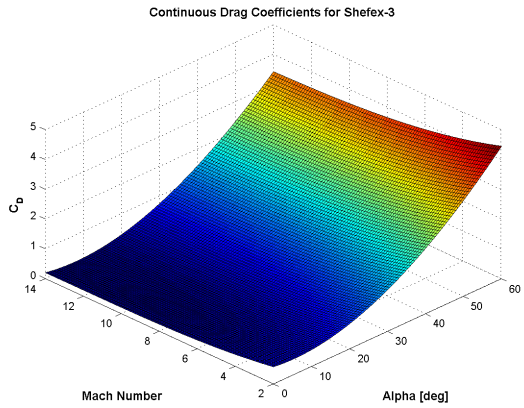

(b) Continuous C_D

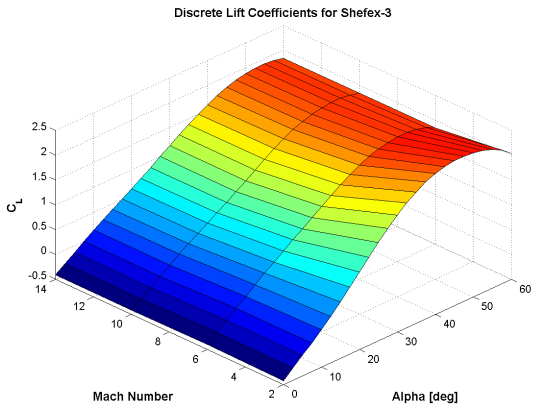

(c) Discrete C_L

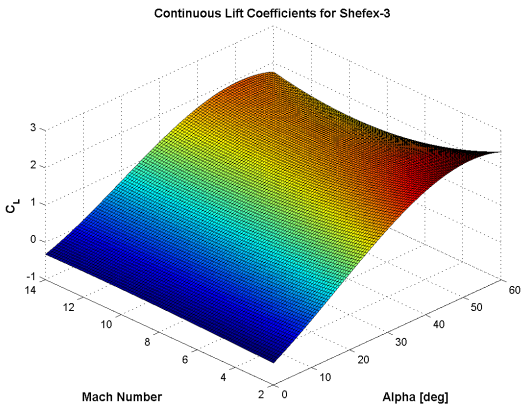

(d) Continuous C_L

Figure 5: Discrete and Continuous Aerodynamic Coefficients

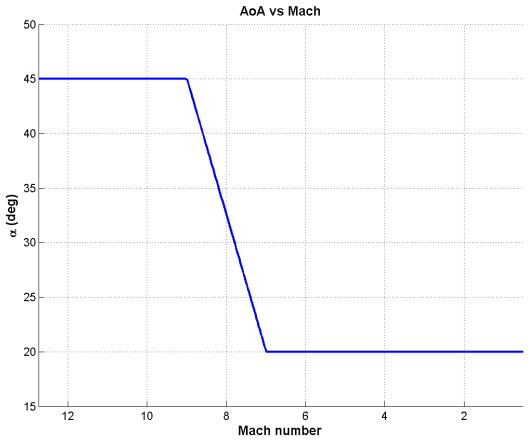

Figure 6: Nominal Angle of Attack Profile

Table 2: Environmental Constraints

Environmental Constraints	Max value
$q(Pa)$	$4 \cdot 10^4$
$\dot{Q}(W/m^2)$	$3.5 \cdot 10^6$
n_z	8

Table 3: Flight Control System Constraints

Constraints	Max value
$\dot{\alpha}(deg/s)$	10
$\dot{\sigma}(deg/s)$	10
$\ddot{\alpha}(deg/s^2)$	4
$\ddot{\sigma}(deg/s^2)$	4

IV. Trajectory Planning - Optimal Control Problem

For the formulation of the optimal-control problem (OCP) representing the guidance, the priority of the mission is the possibility to recover the vehicle. This means that we are interested to minimize the dispersion around the terminal point, meant as the parachute opening interface, having at the same time proper conditions for its deployment. To do this, we need to properly formulate the OCP to be solved. The solution to this problem will provide us the reference solution, that is, the reference trajectory, and the reference controls, which satisfy all our requirements. This is the objective of the trajectory planner. For this specific case, the central gravity field is considered, and the Earth rotation is neglected.

A. Cost function

Minimize the cost function J

$$J = w_\theta(\theta_f - \theta_{ref})^2 + w_\phi(\phi_f - \phi_{ref})^2 \tag{7}$$

subject to the differential equations

$$\begin{aligned}
\dot{h} &= V\sin\gamma \\
\dot{\theta} &= \frac{V\cos\gamma\cos\psi}{r\cos\phi} \\
\dot{\phi} &= \frac{V\cos\gamma\sin\psi}{r} \\
\dot{V} &= -D - g\sin\gamma \\
\dot{\gamma} &= \frac{L\cos\sigma}{V} + \left(\frac{V}{r} - \frac{g}{V}\right)\cos\gamma \\
\dot{\psi} &= \frac{L\sin\sigma}{V\cos\gamma} - \frac{V}{r}\cos\gamma\cos\psi\tan\phi \\
\dot{\sigma} &= u_\sigma
\end{aligned} \tag{8}$$

and to the path constraints

$$\left\{ \begin{array}{c} 0 \\ 0 \\ -n_{z,U} \end{array} \right\} \leq \left\{ \begin{array}{c} q \\ \dot{Q} \\ n_z \end{array} \right\} \leq \left\{ \begin{array}{c} q_U \\ \dot{Q}_U \\ n_{z,U} \end{array} \right\} \tag{9}$$

The states are also bounded

$$\left\{\begin{array}{c} 0 \text{ km} \\ -90^\circ \\ -90^\circ \\ 10 \text{ m/s} \\ -45^\circ \\ -180^\circ \end{array}\right\} \leq \left\{\begin{array}{c} h \\ \theta \\ \phi \\ V \\ \gamma \\ \psi \end{array}\right\} \leq \left\{\begin{array}{c} 120 \text{ km} \\ 90^\circ \\ 90^\circ \\ 7000 \text{ m/s} \\ 30^\circ \\ 180 \end{array}\right\} \tag{10}$$

The conditions for the opening of the parachute give extra constraints on final altitude and speed.

$$\left\{\begin{array}{c} 5 \text{ km} \\ 125 \text{ m/s} \end{array}\right\} \leq \left\{\begin{array}{c} h_f \\ V_f \end{array}\right\} \leq \left\{\begin{array}{c} 10 \text{ km} \\ 185 \text{ m/s} \end{array}\right\} \tag{11}$$

It is worth to notice that the vehicle is not "inertialess". In other words, the controls cannot instantaneously change, but they can only vary with the rate reported in Table 3. Mathematically, this translates into an additional differential equation in the system (8). This additional state is the bank-angle, and the control in this system is its derivative $\dot{\sigma}$.

$$\left\{\begin{array}{c} -89^\circ \\ -10\ ^\circ/\text{s} \end{array}\right\} \leq \left\{\begin{array}{c} \sigma \\ \dot{\sigma} \end{array}\right\} \leq \left\{\begin{array}{c} 89^\circ \\ 10\ ^\circ/\text{s} \end{array}\right\} \tag{12}$$

While limitations on the bank angle and its rate are always taken into account in the transcription with the use of an additional differential equation, the maximum angular acceleration is not. This limit indeed can be easily verified a posteriori, by numerically differentiating the bank angular rate. In case the results exceed the prescribed limits, it can also be included explicitly in the transcription process. However, for all the considered cases here this limit was not violated.

B. Optimality of Solution via Bellman's Principle

In this section we will indirectly verify the optimality of the solution. Indeed, there are different ways to check the optimality of a computed trajectory. The classical methods involve the verification of the KKT conditions or the analysis of the properties of the Hessian matrix associated to the active constraints. A simpler alternative is the application of the Bellman's principle[10,11] , stated as follows.

Bellman's Principle *An optimal policy has the property that whatever the initial state and initial decision are, the remaining decisions must constitute an optimal policy with regard to the state resulting from the first decision.*

In other words, given an optimal solution, having initial and final states $\mathbf{x}(t_0)$ and $\mathbf{x}(t_f)$ respectively, and a cost function $J^* = J(t, \mathbf{x}^*, \mathbf{u}^*)$, if we solve again the same optimal control problem with an initial state $\mathbf{x}(t_m)$

$$\mathbf{x}(t_m) \in \mathbf{x}^*(t),\ t_m \in [t_0, t_f]$$

the new solution will be part of the original solution, and the new cost function J_m will be equal or less to the original one.

Figures 7-9 show the application of the Bellman's principle to the nominal scenario here analysed.

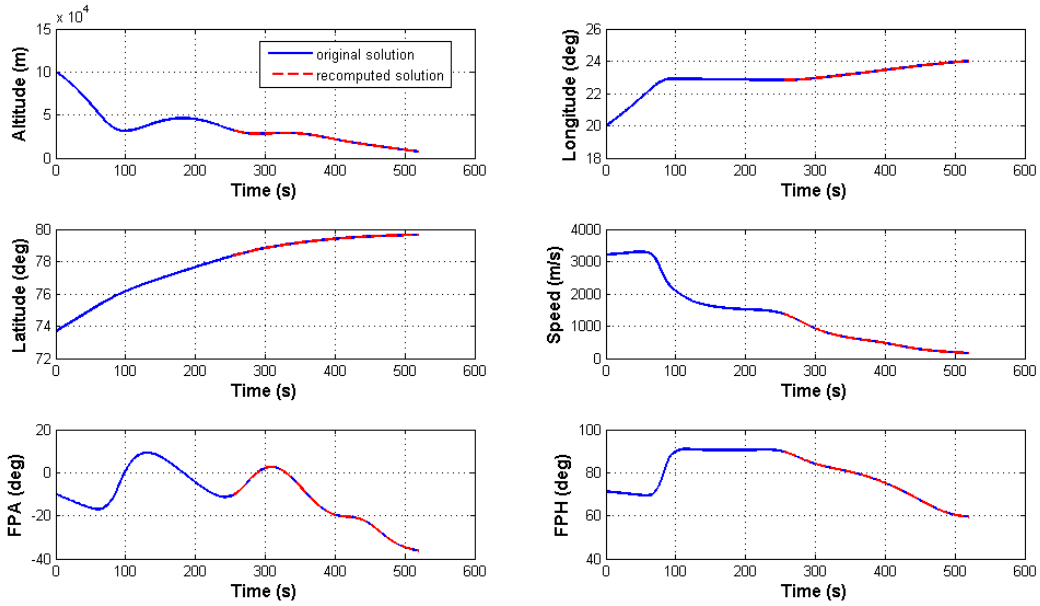

Figure 7: Bellman Optimality Test for Nominal Scenario - States

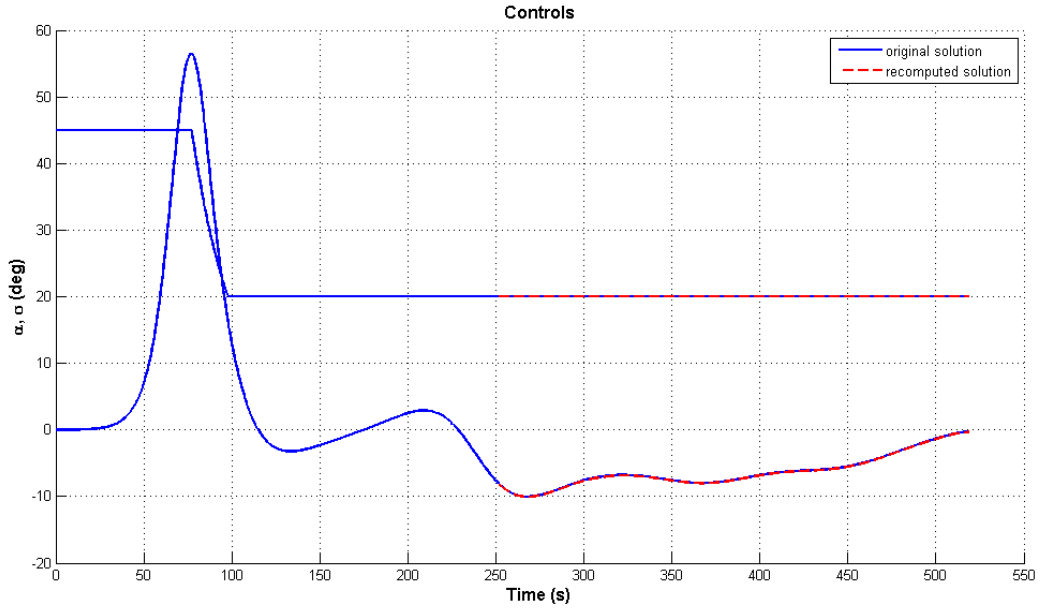

Figure 8: Bellman Optimality Test for Nominal Scenario - Controls

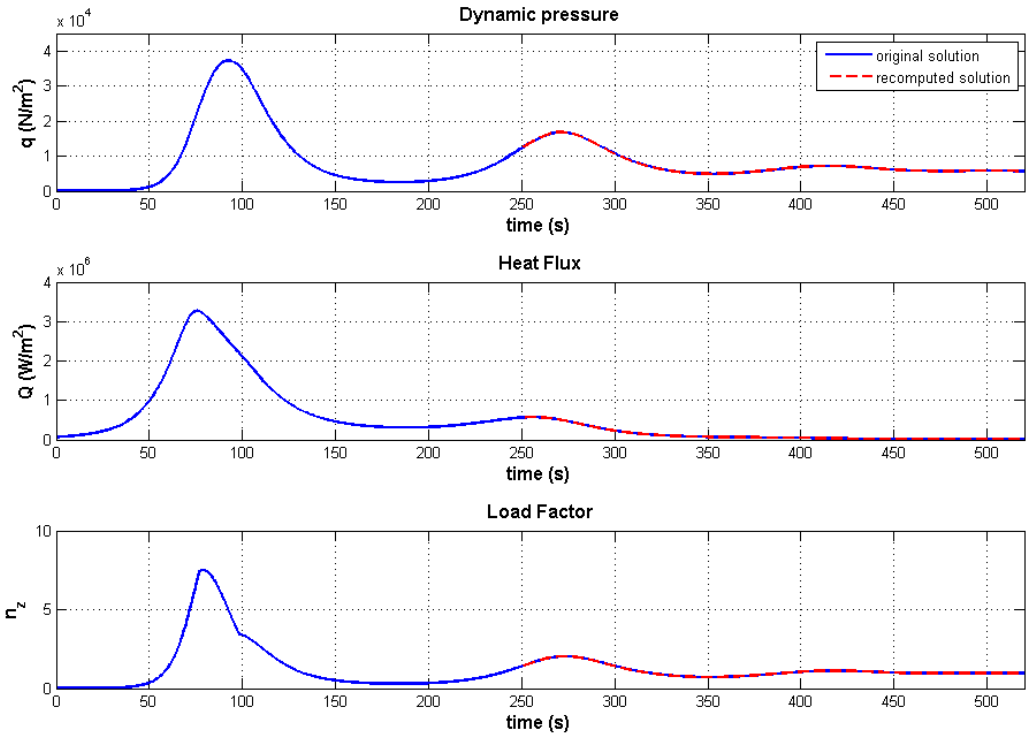

Figure 9: Bellman Optimality Test for Nominal Scenario - Constraints

From the figures 7-9 we can observe how the states, the controls and the constraints computed with the second run (red dotted line) perfectly overlap the states and controls histories previously obtained. This confirms that, since the Bellman Principle holds, the solution found is effectively optimal for the analysed problem.

The condition on the cost function

$$J_m \leq J^* \tag{13}$$

is also satisfied.

V. Trajectory Tracking - LQR Feedback Control

The inflight conditions will be of course different from the nominal path coming from the solution of the optimal control problem. Variations in density, mass, and aerodynamics, for instance, can generate significantly different trajectories. Moreover, errors on initial conditions affect the trajectory as well. It is then necessary to develop a controller to track the nominal trajectory. This can be done using a gain-scheduling approach. The original system is locally linearized and a series of Riccati controllers is synthesized[11,12] . The gains are then linearly interpolated along the trajectory to control the full nonlinear system.

A. Transformation of LTV in LTIs

One of the most common approaches to control LTV systems is the gain scheduling technique. This approach consists of linearizing the initial nonlinear system along the nominal trajectory to extract the state-space representations of the local LTI systems.

$$f(t_k, \mathbf{x}_k, \mathbf{u}_k) \longrightarrow \{\mathbf{A}_k, \mathbf{D}_k, \mathbf{C}_k, \mathbf{D}_k\}\,,\ k = 1, ...N \tag{14}$$

This means that we perform the following differentiation operations.

$$A(i,j)_k = \left.\frac{\partial f_i(t, \mathbf{x}, \mathbf{u})}{\partial x_j}\right|_{\substack{\mathbf{x}=\mathbf{x}_k \\ \mathbf{u}=\mathbf{u}_k}} \tag{15}$$

$$B(i,j)_k = \left.\frac{\partial f_i(t, \mathbf{x}, \mathbf{u})}{\partial u_j}\right|_{\substack{\mathbf{x}=\mathbf{x}_k \\ \mathbf{u}=\mathbf{u}_k}} \tag{16}$$

$$\tag{17}$$

All the states are observable, and no feed-through term is involved in the system, so $\mathbf{C}$ and $\mathbf{D}$, are equal to the identity and zero matrix respectively.

$$\mathbf{C}_k = \mathbf{I}_{N_s,N_s} \tag{18}$$

$$\mathbf{D}_k = \mathbf{O}_{N_s,N_c} \tag{19}$$

$$\tag{20}$$

For the case analysed, the LTV system has been sampled in 100 points along the nominal trajectory, and the Bryson's rule has been used for the computation of the gains[13] . In many literature examples the tracking involves mainly the longitudinal motion, while for the lateral guidance the heading-error control[4,5]) is used. In this case instead, for the region of full rank of matrix $\mathbf{B}$, all the six states can be tracked, and the errors on their final states meet the requirements of the mission. For the synthesis of the controller, the model described in (8) is used.

$$\mathbf{u} = \left\{ \begin{array}{c} \alpha \\ \sigma \end{array} \right\} \tag{21}$$

Once $\mathbf{A}_i$, $\mathbf{B}_i$, $\mathbf{C}_i$, $\mathbf{D}_i$ are computed, the LQR is synthesized. $\mathbf{Q}_i$ and $\mathbf{R}_i$ are set so that the bank angle and the angle of attack modulation are the primary and the secondary controls respectively. The gains are computed using the classical expression coming from the LQR theory[11,12,14] ,

$$\mathbf{K} = \mathbf{R}^{-1}\mathbf{B}^T\mathbf{P} \tag{22}$$

where $\mathbf{P}$ is the solution of the related Algebraic Riccati Equation.

$$\mathbf{A}^T\mathbf{P} + \mathbf{P}\mathbf{A} - \mathbf{P}\mathbf{B}\mathbf{R}^{-1}\mathbf{B}^T\mathbf{P} + \mathbf{Q} = 0 \tag{23}$$

If we define the error state as

$$\mathbf{e}(t) = \mathbf{x}(t) - \mathbf{x}_{ref}(t) \tag{24}$$

we can use the classical MIMO feedback control law.

$$\mathbf{u}_c = -\mathbf{K} \cdot \mathbf{e}(t) \tag{25}$$

The region where the feedback controller can be effectively applied is associated to the property of almost strictly passivity[15] . In other words, the matrix $\mathbf{B}$ of the linearized system becomes rank-deficient when the bank angle approaches 0. From the physical point of view, this translates into a lack of vehicle's control authority. To prevent this, and to guarantee to the vehicle sufficient control authority needed, the classical equilibrium glide condition is modified as follows.

$$U_v = L\cos\sigma + \frac{V^2}{r} - g \geq U_{min} \tag{26}$$

For the considered scenario, U_{min} is set equal to 25 m/s^2. With this choice, the risk to reach the condition $\sigma = 0°$ is excluded. These limitations are indeed consequence of the non-standard entry conditions (smaller speed V, steeper flight-path angle γ w.r.t. nominal entry conditions[4,5]). The adopted feedback guidance scheme is reported in Figure 10. We can see that the proposed scheme is made by two parts: an *offline* and

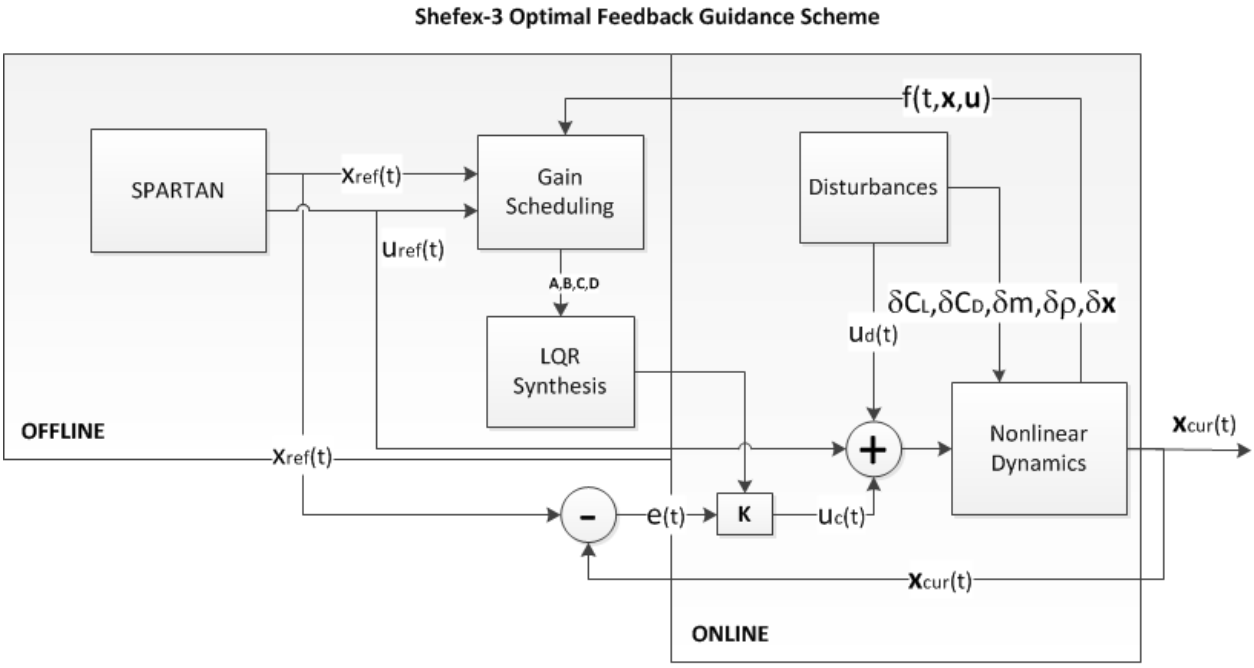

Figure 10: Feedforward-Feedback Guidance Scheme

an *online* section. In the offline section, the reference trajectory and the nominal controls are generated. They are processed to extract the LTI systems for the synthesis of the tracking controllers. This data is used online in combination with the nonlinear dynamics and the disturbances to validate the controller via MonteCarlo campaign.

VI. Nominal Trajectory

The Simulations have been performed using SPARTAN, a tool developed by DLR based on the use of PseudoSpectral Methods[16] for the transcription of optimal control problems[17,18] . All optimal control problems have been discretized using sets between 50 and 125 nodes for the proper generation of the related NLP problem, solved with SNOPT[19] . Figures 11 - 13 show the reference states and controls, as well as the constraints and the groundtrack.

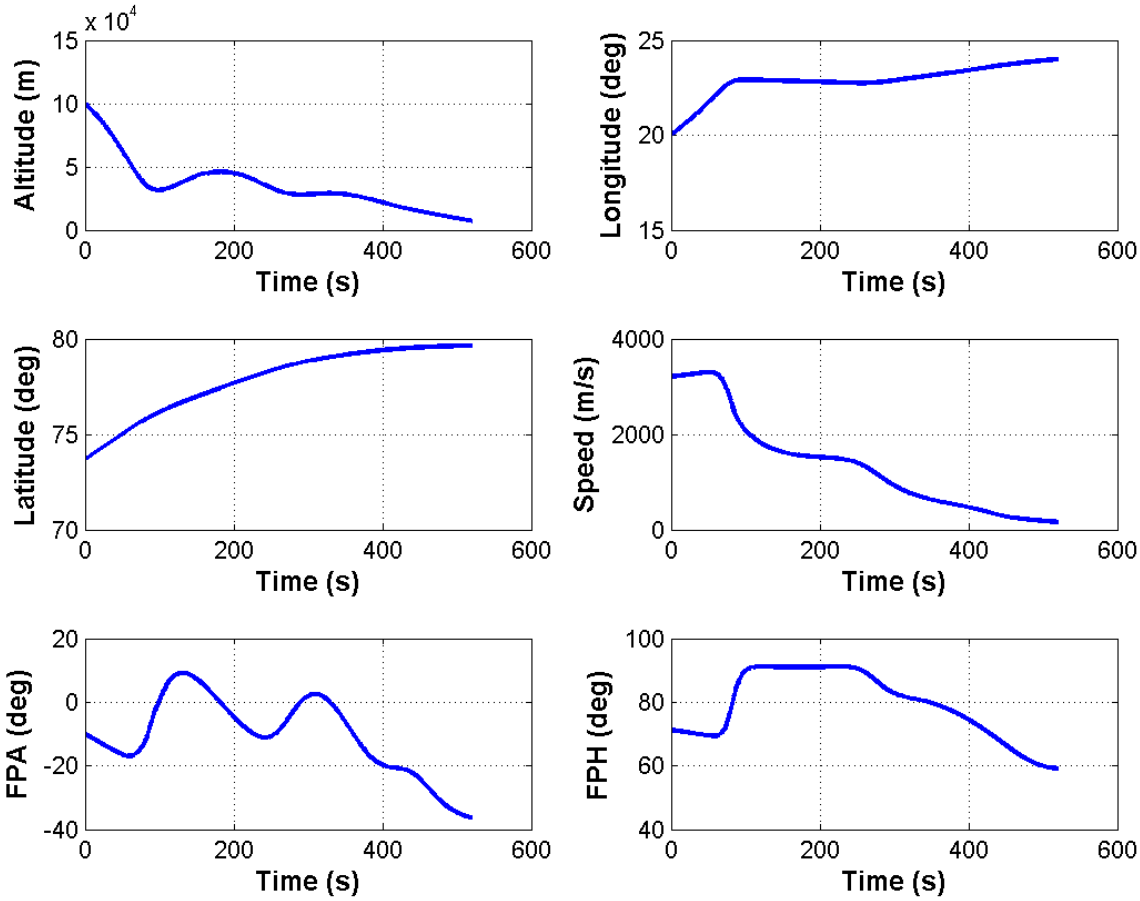

Figure 11: Nominal Scenario: States

It is possible to observe an initial skip entry due to the highly negative flight-path angle combined with the speed. Accordingly to these conditions, we find the peaks for the constraints acting on the spacecraft (dynamic pressure, heat flux and load factor). The computed trajectory fullfills all the constraints defined in the OCP, and drives the vehicle to the prescribed terminal point.

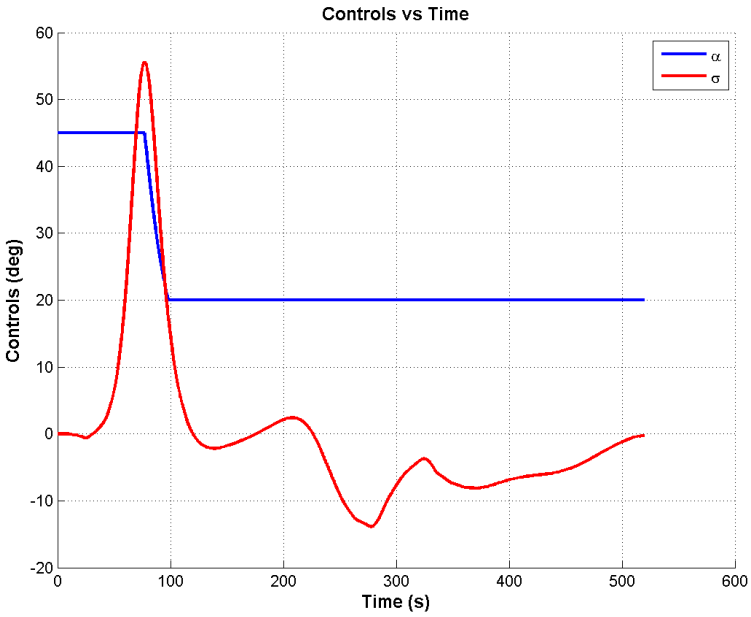

Figure 12: Nominal Scenario: Controls

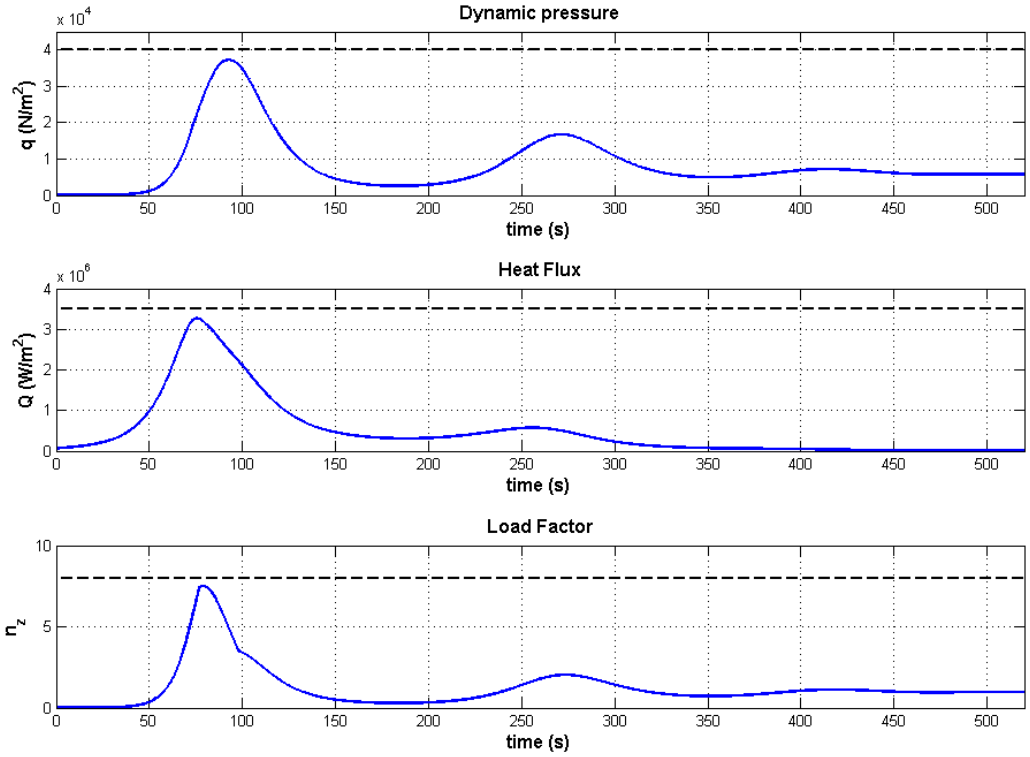

Figure 13: Nominal Scenario: Constraints

VII. Simulation Campaign

To test the controller, a campaign of 100 simulations has been performed. Systematic variations on mass, both aerodynamic coefficients and density of the atmosphere have been considered, and dispersions on the initial position and velocity have been included too. These uncertainties are summarized in Table 5, and the results reported in Figures 14 - 18.

Table 4: Dispersions for the MonteCarlo campaign

Variable	Dispersion Range
h	$\pm 500\ m$
θ	$\pm 0.02°$
ϕ	$\pm 0.02°$
V	$\pm 50\ m/s$
γ	$\pm 0.5°$
ψ	$\pm 0.05°$
m	$\pm 1\%$
C_L	$\pm 20\%$
C_D	$\pm 20\%$
ρ	$\pm 20\%$

Uncertainties on initial conditions have been selected on the basis of the experience matured with SHEFEX-2. Mass uncertainty comes from the results of the mass budget generated during the SHEFEX-3 Cuncurrent Engineering study that took place in the CEF (Cuncurrent Engineering Facility) at the DLR Institute of Space Systems in Bremen in October 2013. Aerodynamic uncertainties have been suggested by DLR aerodynamics experts[20] who generated the database, while the uncertainty on the atmospheric density is compatible with the ranges associated to more complex models such as US76 or NRLMSISE-00.

On top of these perturbations, other effects have been included. White noise with limited bandwidth has been added to simulate the effects of the navigation. The effects of the discretization have been taken into account as well, having the solution running at 10 Hz. Moreover, a delay in the execution of the commands of 1 s has been introduced, in order to compensate for the inner dynamics handled by the attitude controller. The selection of these values has been performed after several discussions with the responsibles for SHEFEX-3 Navigation and Attitude Control subsystems[20] .

Table 5: Effects modeled for the MonteCarlo campaign

Effect	Value
noise on h	$1\ m\ (1\sigma)$
noise on θ	$0.0001°\ (1\sigma)$
noise on ϕ	$0.0001°\ (1\sigma)$
noise on V	$0.1 m/s\ (1\sigma)$
noise on γ	$0.001°\ (1\sigma)$
noise on ψ	$0.001°\ (1\sigma)$
delay	$1\ s$
frequency	$10\ Hz$

It is possible to observe how the effect of the Feedback Controller allows to meet the requirements on the final points for all the considered cases, while the use of the sole feedforward guidance does not ensure to satisfy always the desired entry conditions. Indeed, Figure 14 shows the states obtained with open-loop (in red) and closed-loop (in green) simulations. A more detailed view can be obtained by the analysis of the

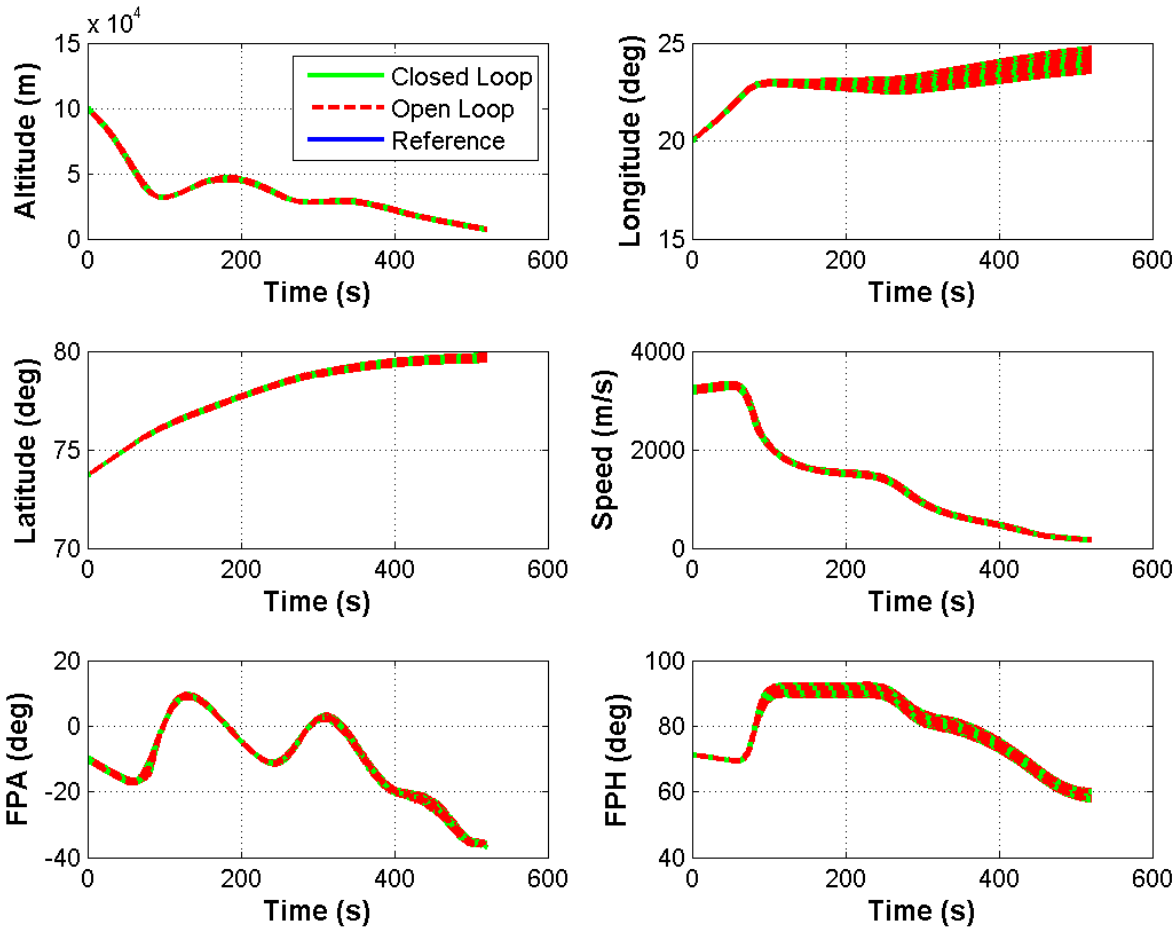

Figure 14: MonteCarlo Simulation: States

Figure 15, where the state errors w.r.t. the nominal solutions are reported. It is clearly visible how the error on the terminal states is significantly reduced with the use of the tracking controller, and does not exceed the prescribed limits, represented by the dot lines.

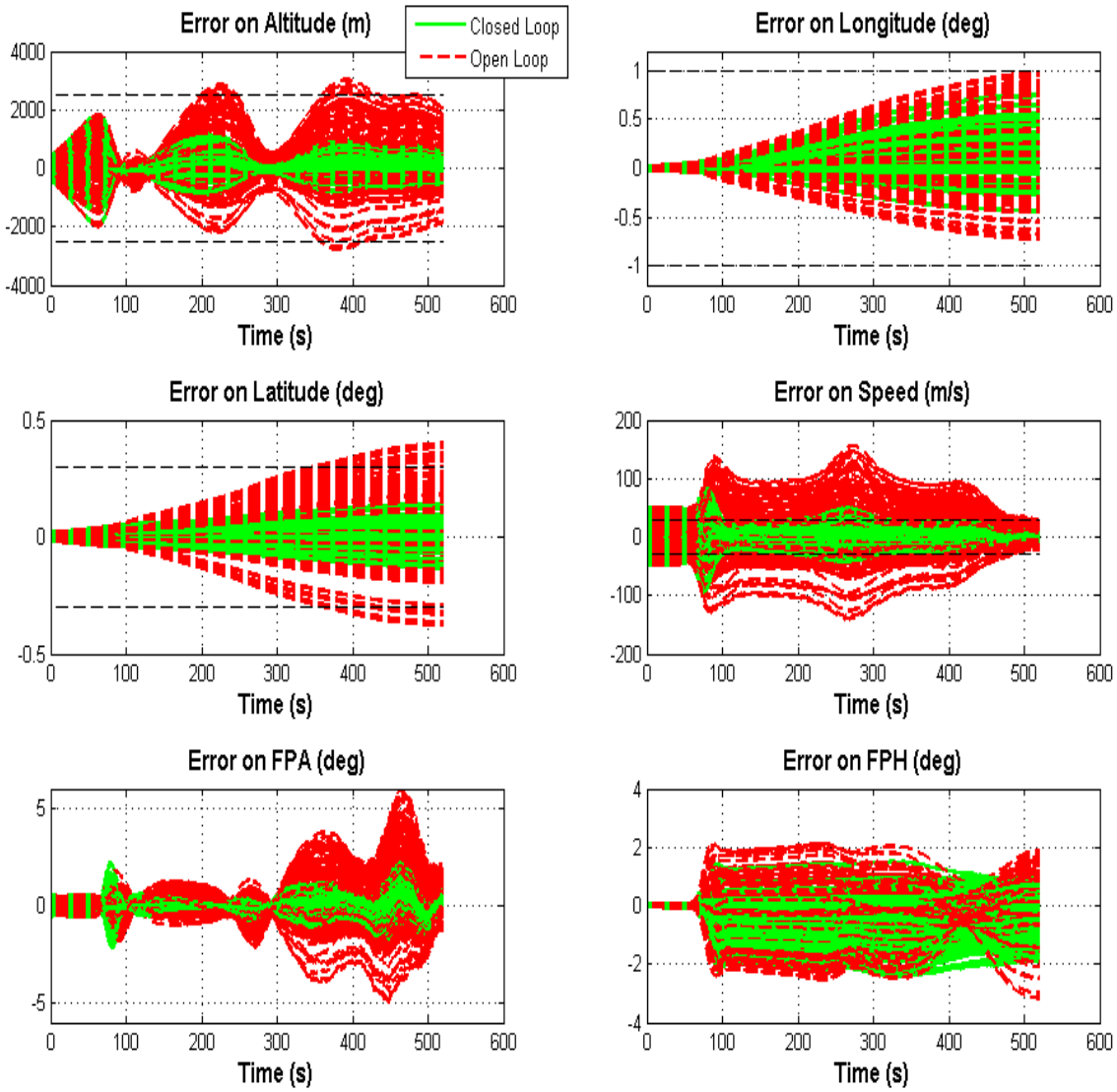

Figure 15: MonteCarlo Simulation: Errors on States

In Figure 16 we can observe how the tracker uses mainly modulations in terms of bank-angle, and only small adjustements of the angle of attack are permitted. Specifically, the maximum observed variation of the angle of attack w.r.t. the nominal profile is, in absolute value, less than 2°. In terms of constraints (Figure 17), no violations of the maximum values have been found when the tracker was used. Higher peaks could be observed, especially for the load factor, but they are mainly a consequence of worse initial conditions, and are limited by the tracker in the limits of the constraints of the scenario. In some cases, the open-loop trajectories exceed the maximum value of the dynamic pressure, while the feedback action is strong enough to avoid violations. Similar conclusions can be drawn for the mission terminal point (Figure 18). While for the open-loop simulations, some trajectories ended outside the prescribed terminal area, with the use of the feedback controller, all of the analysed cases fell in the allowed terminal ellipse.

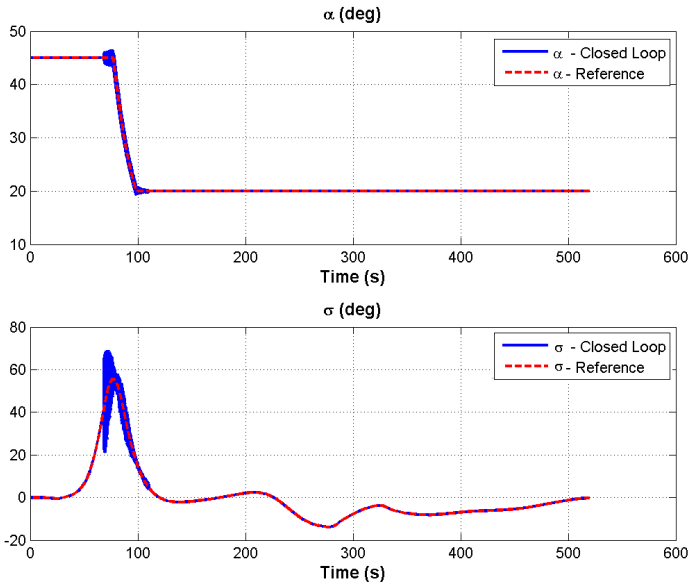

Figure 16: MonteCarlo Simulation: Controls

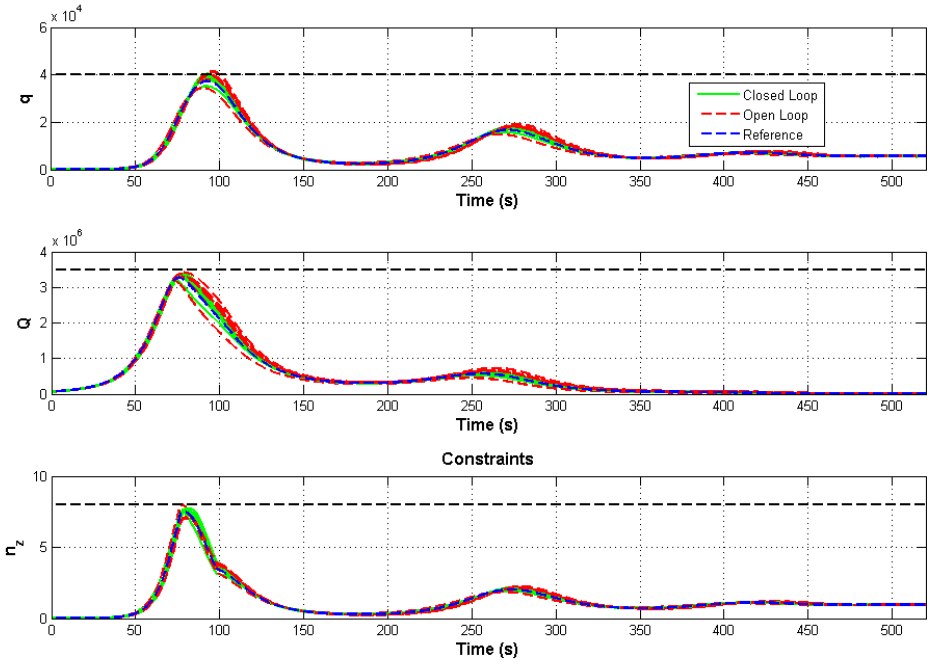

Figure 17: MonteCarlo Simulation: Constraints

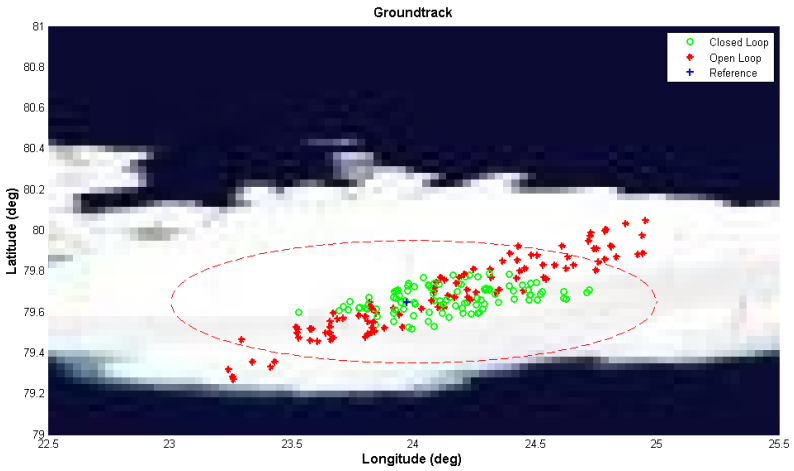

Figure 18: MonteCarlo Simulation: Terminal Points

Future Development

During the real mission, bigger or further uncertainties may affect the performances of the real system, and some models may not reflect adequately the inflight conditions. For these reasons, future developments will include the use of more complex environmental models, such as the NRLMSISE-00, and the use of wind-gusts models in the analysis. Moreover, the replacement of the Gain-Scheduling LQR with more robust linear or nonlinear tracking control methodologies like Sliding Mode Control, or Gain-Scheduling H_∞ is under consideration. A possible realization of this improved guidance scheme is reported in Figure 19, and is at the moment subject to investigation.

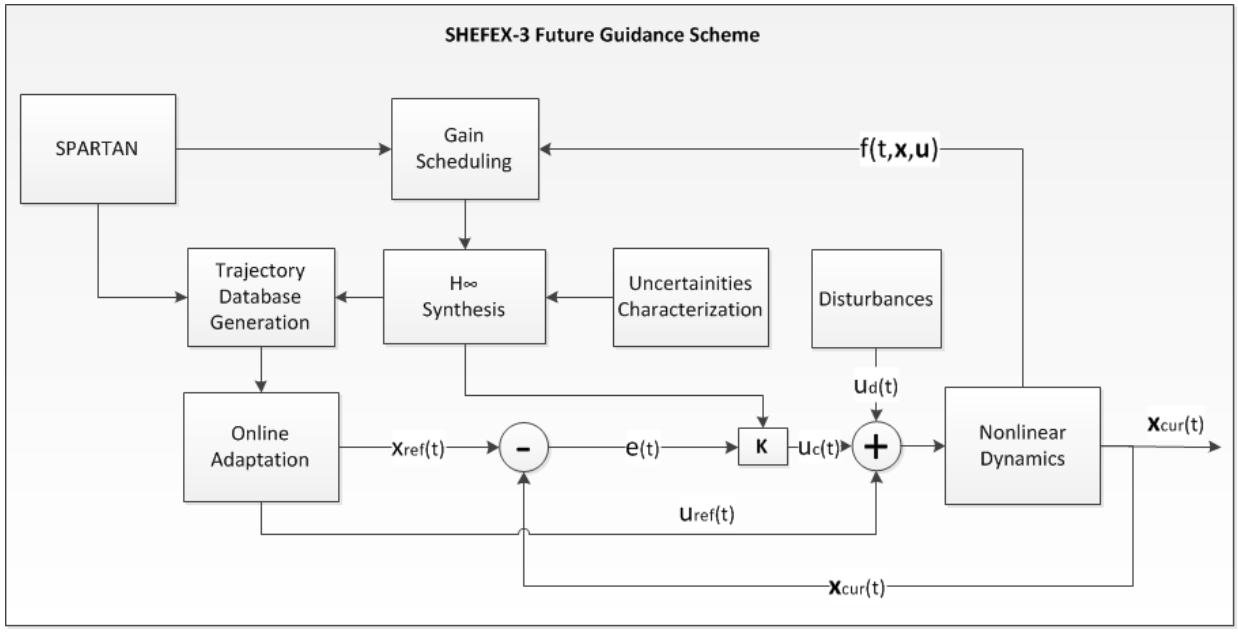

Figure 19: Improved Feedforward-Feedback Guidance Scheme

Conclusions

In this work the results obtained with the use of PseudoSpectral Methods have been coupled with a Gain-Scheduling LQR technique to ensure that the requirements on the terminal points for SHEFEX-3 scenario are satisfied. The non-standard entry conditions, together with the constraints on the angle of attack, reduce the use of the tracking controller to the range where satisfactory control authority can be ensured. This approach has been analysed including environmental dispersions, vehicle's uncertainties, perturbed initial conditions as well as navigation and attitude control effects, such as delays and bandwidth limited white noises. Results show that the proposed approach can drive the vehicle towards the terminal points within the prescribed limits for all of the simulated cases. For instance, in their respective worst-cases, the errors on final altitude, speed, longitude and latitude were reduced by 71.3%, 71.2%, 23.6%, and 65.0% respectively. However, as stated in the previous section, the inflight conditions may be affected by further uncertainties and / or disturbances. For this reason, to ensure the success of the mission, more robust control techniques are at the moment investigated, together with the use of adaptive feedforward guidance schemes.

References

[1]Steffes S. R., "Development and Analysis of SHEFEX-2 Hybrid Navigation System Experiment", Fachbereich Produktionstechnik, Universität Bremen, Bremen, 2012

[2]Steffes S. R., "Real-Time Navigation Algorithm for the SHEFEX2 Hybrid Navigation System Experiment,",*Proceedings of the AIAA Guidance, Navigation, and Control Conference*, Minneapolis, 2013

[3]Samaan M., Theil S., "Development of a low cost star tracker for the SHEFEX mission,",*AEROSPACE SCIENCE AND TECHNOLOGY*, Vol.23 No. 1, 2012

[4]Mease, K. D., Chen D. T., Teufel P., Schöneberger H., "Reduced-Order Entry Trajectory Planning for Acceleration Guidance",*Journal of Guidance, Control and Dynamics*, Vol.25 No. 2, March-April 2002

[5]Lu P., Hanson J. M., "Entry Guidance for the X-33 Vehicle",*Journal of Spacecraft and Rockets*, Vol.35 No. 3, May-June 1998

[6]Daum A., "Solutions to Problems in the optimization of Performance of Reusable Aeroassisted Orbital Transfer System," ESA Technical Translation of Ph.D. Dissertation, Institute for Chemical Propulsion and Engineering., Lampoldshausen, Germany, , 1995.

[7]Department of Defense, "World Geodetic System 1984, Its Definition and Relationships With Local Geodetic Systems", Technical Report, 3rd ed., January 2000

[8]Gallais P., *Atmospheric Re-Entry Vehicle Mechanics*, Springer-Verlag, New York, 2007

[9]Bollino K. P., "High-Fidelity Real-Time Trajectory Optimization for Reusable Launch Vehicles", Ph.D. Dissertation, Mechanical and Astronautical Engineering Dept., Naval PostGraduate School., 2006

[10]Bellman R., *Dynamic Programming*, Princeton University Press, 1957

[11]Lavretsky E., Wise. K., *Robust and Adaptive Control: With Aerospace Applications*, Springer-Verlag, New York, 2012

[12]Skogestad S., Postlethwaite I., *Multivariable Feedback Control: Analysis and Design, 2nd ed.*, Wiley-Interscience, 2005

[13]How J. P., Frazzoli., E., "Feedback Control Systems",*Massachusetts Institute of Technology OpenCourseWare*, http://ocw.mit.edu/courses/aeronautics-and-astronautics/16-30-feedback-control-systems-fall-2010 (Accessed 6 Jan, 2014). License: Creative Commons BY-NC-SA

[14]Mooij, E., *Linear Quadratic Regulator Design for an Unpowered, Winged Re-entry Vehicle*, Delft University Press, Delft, 1998

[15]Mooij, E., "Passivity Analysis for Non-Linear, Non-Stationary Entry Capsules: Translational Motion",*18th IFAC World Congress*, Milan, 2011.

[16]Garg, D., "Advances in Global PseudoSpectral Methods for Optimal Control," Ph.D. Dissertation, Department of Mechanical and Aerospace Engineering., University of Florida, FL, 2011.

[17]Sagliano, M., Theil S., "Hybrid Jacobian Computation for Fast Optimal Trajectories Generation",*AIAA Guidance, Navigation, and Control (GNC) Conference*, AIAA 2013-4554, Boston, MA, 2013, doi:10.2514/6.2013-4554

[18]Sagliano, M., "Performance analysis of linear and nonlinear techniques for automatic scaling of discretized control problems",*Operations Research Letters*, Volume 42, Issue 3, May 2014, Pages 213-216, doi: 10.1016/j.orl.2014.03.003

[19]Gill, P. E., Murray W., Saunders M. A., "User's Guide for SNOPT Version 7: Software for Large-Scale Nonlinear Programming"', Software User Manual, Department of Mathematics, University of California, San Diego, CA, 2008

[20]VV.AA., "SHEFEX-3 Progress meetings", Stuttgart, Bremen, 2013-2014